# Effect of wall friction on shock-flame interactions in a hydrogen-air mixture

**Shen, Ting[1], Xiao, Huahua[1, 2, *]**
**1 State Key Laboratory of Fire Science, University of Science and Technology of China, Hefei, 230027, China, ssharon@mail.ustc.edu.cn**
**2 Dalian National Laboratory for Clean Energy, Dalian, 116023, China, xiaoh@ustc.edu.cn**

## ABSTRACT

Shock-flame interactions (SFI) occur in a variety of combustion scenarios of scientific and engineering interest, which can distort the flame, extend the flame surface area, and subsequently enhance heat release. This process is dominated by Richtmyer-Meshkov instability (RMI) that features the perturbation growth of a density-difference interface (flame) after the shock passage. The main mechanism of RMI is the vorticity deposition results from a misalignment between pressure and density gradients. This paper focuses on the multi-dimensional interactions between shock wave and flame in a hydrogen-air mixture. The simulations of this work were conducted by solving three-dimensional fully-compressible, reactive Navier-Stokes equations using a high-order numerical method on a dynamically adapting mesh. The effect of wall friction on the SFI was examined by varying wall boundary condition (free-slip/no-slip) on sidewall. The results show that the global flame perturbation grows faster with the effect of wall friction in the no-slip case than that in the free-slip case in the process of SFI. Two effects of wall friction on SFI were found: (1) flame stretching close to the no-slip wall, and (2) damping of local flame perturbation at the no-slip wall. The flame stretch effect leads to a significantly higher growth rate in the global flame perturbation. By contrast, the damping effect locally moderates the flame perturbation induced by RMI in close proximity to the no-slip wall because less vorticity is deposited on this part of flame during SFI.

**Keywords:** Shock-flame interaction; Richtmyer-Meshkov instability; Vorticity; Wall friction; Baroclinic torque; Numerical simulation

## 1 INTRODUCTION

Shock-flame interactions occur in a variety of combustion scenarios of scientific and engineering interest, including supernova explosions [1-4], space propulsion [5-7], and industrial explosions [8-10]. A large number of experiments and numerical simulations [11-19] were conducted to study shock-flame interactions. These studies suggest that shock waves interacting with a flame can distort the flame, extend the flame surface area, and subsequently enhance energy release. Moreover, shock-flame interactions play an important role in the onset of deflagration-to-detonation transition (DDT) [14, 20-24].

Previous studies show that flame distortion induced by the interaction of a single-mode flame and shock wave is close to laminar flamelet regime [13, 25]. The fundamental mechanism during this process is the Richtmyer-Meshkov instability (RMI) that is generally created at the interface between two fluids of different densities [26, 27]. A kind of physically acceptable viewpoint to understand the RMI evolution from Zabusky et al. [28, 29] is on the basis of vortex dynamics. Vorticity is deposited at the interface through baroclinic torque when there is a misalignment between pressure and density gradients ($\Delta\rho \times \Delta p$) [28-33]. This leads to growth of interface perturbation. Interactions between shock and single-mode perturbated inert interface were extensively studied, and different effective models were proposed to describe the growth of RMI [12, 26, 34]. For chemically reacting flows such as flames, the main features and mechanism of flame perturbation were found to be similar to those of inert RMI [13, 25]. The effect of shock strength, perturbation amplitude, and wavelength has been examined [13, 17]. On the basis of inert growth model of RMI, Yang and Radulescu [17] recently suggested a model for describing the flame perturbation development.

Wall friction generally can play an important role in the dynamics of flame [35, 36] and shock wave [37-39] in practical systems. Wall friction in the presence of viscosity can have an effect on the generation/amplification of acoustic and shock waves [35, 36, 40-43]. Interactions between wall

friction and shock wave could induce boundary layer behind shock [37-39]. Wall friction was considered in the processes of shock reflection and interaction with flame using the multi-dimensional computations [20, 38, 39]. They showed that development of lamda-shock as a result of wall friction facilitates shock-flame interaction and DDT. However, the influence of the wall friction on the development of RMI induced by shock-flame interactions received less attention since these studies were mainly focused on the effect of boundary layer on detonation initiation. Yang and Radulescu [17] speculated in their experimental analysis that wall friction may play a role in the flame deformation induced by RMI in the process of shock-flame interactions, but there was a lack of definitive proof. Overall, complete understanding of the effect of wall friction on shock-flame interaction has yet to be obtained, especially for 3D RMIs.

The purpose of this paper is to study the effect of wall friction on shock-flame interactions, especially on the induced RMI. This study is done by solving the 3D fully-compressible reactive Navier-Stokes equations using a high-order numerical algorithm and adaptive mesh refinement.

## 2 NUMERICAL METHOD AND PHYSICAL MODEL

The fully-compressible, reactive 3D Navier-Stokes equations are adopted to simulate the reactive flow [44]:

$$\frac{\partial \rho}{\partial t} + \frac{\partial (\rho u_i)}{\partial x_i} = 0, \tag{1}$$

$$\frac{\partial}{\partial t}(\rho u_i) + \frac{\partial}{\partial x_j}(\rho u_i u_j) = -\frac{\partial p}{\partial x_i} + \frac{\partial \tau_{ij}}{\partial x_j}, \tag{2}$$

$$\frac{\partial (\rho E)}{\partial t} + \frac{\partial (\rho u_j E + p u_j)}{\partial x_j} = \frac{\partial}{\partial x_j}\left(K \frac{\partial T}{\partial x_j}\right) + \frac{\partial (\tau_{ij} u_i)}{\partial x_j} + \rho q \omega, \tag{3}$$

$$\frac{\partial}{\partial t}(\rho Y) + \frac{\partial}{\partial x_i}(\rho Y u_i) = -\frac{\partial}{\partial x_i}\left(\rho D \frac{\partial Y}{\partial x_i}\right) + \rho \omega, \tag{4}$$

$$p = \rho R T / M, \tag{5}$$

$$\tau_{ij} = \rho \nu \left[\left(\frac{\partial u_i}{\partial x_j} + \frac{\partial u_j}{\partial x_i}\right) - \frac{2}{3}\frac{\partial u_k}{\partial x_k}\delta_{ij}\right], \tag{6}$$

$$E = \frac{p}{\rho(\gamma-1)} + \frac{1}{2}u_i^2, \tag{7}$$

where $\rho$ – density, kg/m$^3$; $Y$ – mass fraction of reactant; $u_i$ – $i$th component of the velocity, m/s; $D$ – mass diffusion coefficient, m$^2$/s; $\omega$ – reaction rate, s$^{-1}$; $p$ – pressure, Pa; $\tau_{ij}$ – viscous stress tensor, kg/(m·s$^2$); $E$ – energy, J/kg; $K$ – thermal conductivity, J/(m·s·K); $q$ – chemical heat release, J/kg; $M$ – molecular weight, g/mol; $R$ – universal gas constant, J/(mol·K); $\nu$ – kinematic viscosity, m$^2$/s; $\delta_{ij}$ – unit tensor, $\gamma$ – specific heat ratio.

The simplified, calibrated chemical-diffusive model (CDM) [45, 46] is used to model the reaction,

$$\frac{dY}{dt} \equiv \omega = -A\rho Y \, exp(-E_a/RT), \tag{8}$$

where $A$ – pre-exponential factor, m$^3$/(kg·s); $E_a$ – activation energy, kJ/mol. The kinematic viscosity ($\nu$), mass diffusivity ($D$), and thermal diffusivity ($\alpha$) are dependent upon temperature [46, 47],

$$\nu = \frac{\nu_0 T^{0.7}}{\rho}, D = \frac{D_0 T^{0.7}}{\rho}, \alpha = \frac{K}{\rho C_p} = \frac{\kappa_0 T^{0.7}}{\rho}, \tag{9}$$

where $\nu_0$, $D_0$, and $\kappa_0$ are constants. The input parameters of CDM and computed flame properties for the stoichiometric hydrogen-air mixture initially at 294 K and 17.24 kPa are summarized in Table 1. These initial conditions model the experiments of Yang and Radulescu [17]. The computed flame properties matches those calculated using Cantera python library [48] with a detailed reaction mechanism of Burke et al. [49].

Table 1. Input model parameters and output flame properties for stoichiometric hydrogen and air initially at 17.24 kPa and 294 K.

| Input parameters | | |
|---|---|---|
| $\gamma$ | 1.1648 | Specific heat ratio |
| $M$ | 24.2 g/mol | Molecular weight |
| $A$ | $1.332 \times 10^8$ m³/(kg·s) | Pre-exponential factor |
| $E_a$ | 33.24 $RT_0$ | Activation energy |
| $q$ | 48.70 $RT_0/M$ | Heat release |
| $\nu_0 = D_0 = \kappa_0$ | $3.648 \times 10^{-6}$ kg/(s·m·K$^{0.7}$) | Transport constants |
| Combustion properties | | |
| $S_l$ | 1.97 m/s | Laminar burning velocity |
| $T_b$ | 2320 K | Adiabatic flame temperature |
| $\delta_L$ | 0.375 cm | Laminar flame thickness |
| $\rho_0$ | 0.1707 kg/m³ | Unburned gas density |

Figure 1 shows the schematic computational configuration with dimensions of 53.06 cm × 3.79 cm × 0.95 cm ($L_x \times L_y \times L_z$). The configuration corresponds to a quarter of one flame cell in the experiments of Yang and Radulescu [17, 20]. To achieve that, symmetry boundary conditions are applied at $z = 0$, $y = 0$, and $y = L_y$. Non-reflecting boundary condition is used at $x = 0$ and $L_x$. To investigate the effect of wall friction on shock-flame interactions, two different types of wall boundary conditions (BCs) are considered at $z = L_z$: (1) adiabatic no-slip BC (no-slip case) and (2) adiabatic free-slip (free-slip case).
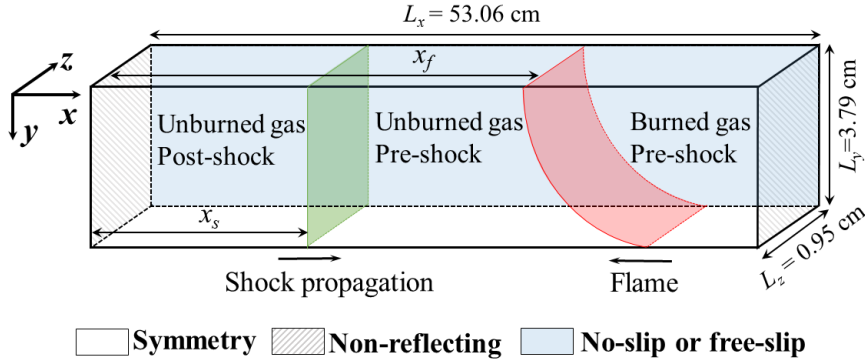


Figure 1. A snapshot of three-dimensional (3D) computational domain.

An incident shock is set initially at a distance of $x_S = 0.2$ cm from the left boundary. Between the left boundary and the shock, there is a uniform flow with the post-shock parameters determined from the Rankine-Hugoniot conditions for a shock with a given Mach number, $M_S = 1.9$ (corresponding to the experiment). The flame is placed ahead of the shock, at a distance $x_f = 27.205$ cm from the left boundary. The initial flame front is assumed partially cylindrical to simulate a 1/4 of a sine wave (wavelength $\lambda = 4L_y$) corresponding to experiment configuration by Yang [17], and is defined with the flame coordinates $(x, y)$,

$$x = (x_f + L_y) - \sqrt{L_y^2 - y^2},\qquad(10)$$

A fifth-order WENO scheme with HLLC Riemann explicit solver [56] is used to solve the governing equations. The time integration is advanced by using a third-order Runge-Kutta algorithm [37, 40]. The computational grid is dynamically refined using adaptive mesh refinement [57]. The refinement criterion is obtained based on the maximum error for each grid cell, $e_{ij}$ = max ($\varphi_x$, $\varphi_y$, $\varphi_{xy}$, $\varphi_{yx}$), in $x$, $y$, and both diagonals [47] where

$$\varphi_x = \frac{|\rho_{i-1,j} - 2\rho_{i,j} + \rho_{i+1,j}|}{0.03|\rho_{i,j}| + |\rho_{i+1,j} - \rho_{i-1,j}|},\qquad(11)$$

3

The quantities $\varphi y$, $\varphi xy$, $\varphi yx$ are calculated similarly. In order to refine the regions with strong shear flows and boundary layers, an additional criterion using a gradient of velocity is given $\|\nabla \vec{u}\|_1$. A cell is tagged for refinement if $e_{ij} > \varepsilon_{ref}$ or $\|\nabla \vec{u}\|_1 > TVGGR$, where $\varepsilon_{ref} = 0.3$ and $TVGGR = 1 \times 10^4$ is the threshold of velocity gradient for grid refinement. Grid resolution tests show that the calculation is converged at $dx_{min} = 0.006$ cm. Thus, the results of this work will be presented for this minimum grid size, corresponding to 63.24 cells per flame thickness at the initial conditions.

Figure 2 shows the (a) numerical and (b) experimental [17] flame perturbation ($\eta$) as a result of shock-flame interaction. Figure 3 compares the numerical simulations and the experiment. The value of the $\eta$ (simulation) corresponds to the experimental measurement of $\eta$. The present numerical results for $\eta$ show a good agreement with the experimental observations $\eta$ by Yang and Radulescu [17], as shown in Fig. 3.
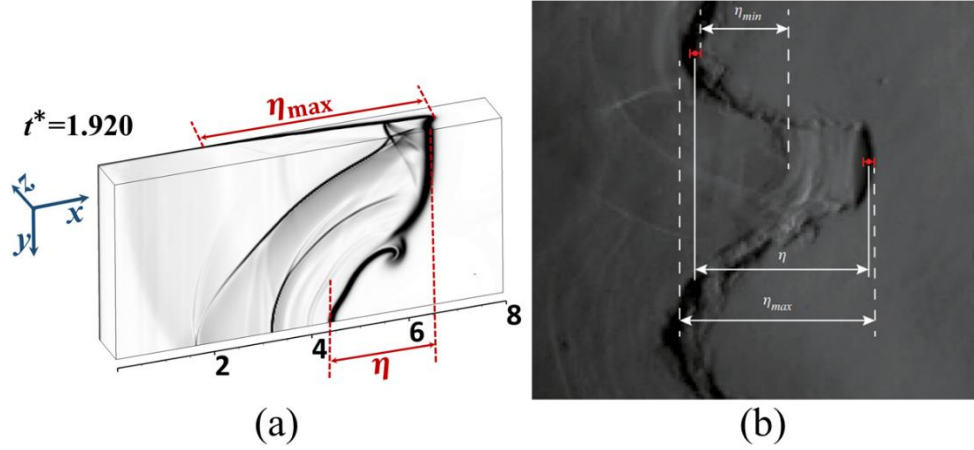


Figure 2. (a) 3D schlieren image of the flame after shock passage in the no-slip case (no-slip BC is set at $z = L_z$) and (b) measurement of the amplitude $\eta$ in the experiment by Yang and Radulescu [17]. Two types of the perturbation were calculated in the computations: (1) $\eta$, the amplitude of flame perturbation at the slice of $z = 0$ (corresponding to that in the experiment), and (2) $\eta_{max}$, the maximum perturbation amplitude of flame in the entire computational domain (as it will be discussed below).
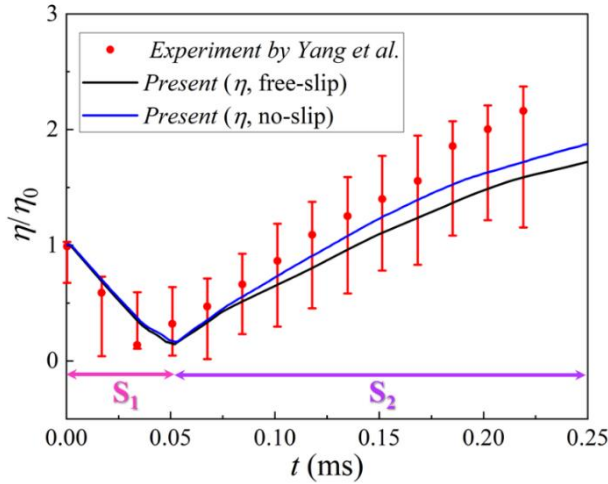


Figure 3. Comparison of the present simulation and the experiment by Yang and Radulescu [17]. $\eta_0$ is the initial amplitude of the flame.

# 3 RESULTS AND DISCUSSION

## 3.1 Development of flame perturbation

Figure 4 shows the time evolution of flame perturbation after the passage of a shock wave with a Mach number of 1.9 in (a) free-slip case and (b) no-slip case. The time was normalized by the characteristic time of the shock passing through the flame, $t^* = t/(\eta_0/V_S)$, where $\eta_0$ is the amplitude of the flame before shocked and $V_S = 651.7$ m/s is the shock speed. The images in the first row show the state of incident shock wave and flame front just before the shock arrives at the flame in the two cases. The flame perturbation ($\eta$) can be divided into two stages, i.e., shock compression ($S_1$) and perturbation growth stages ($S_2$), as shown in Fig. 3.
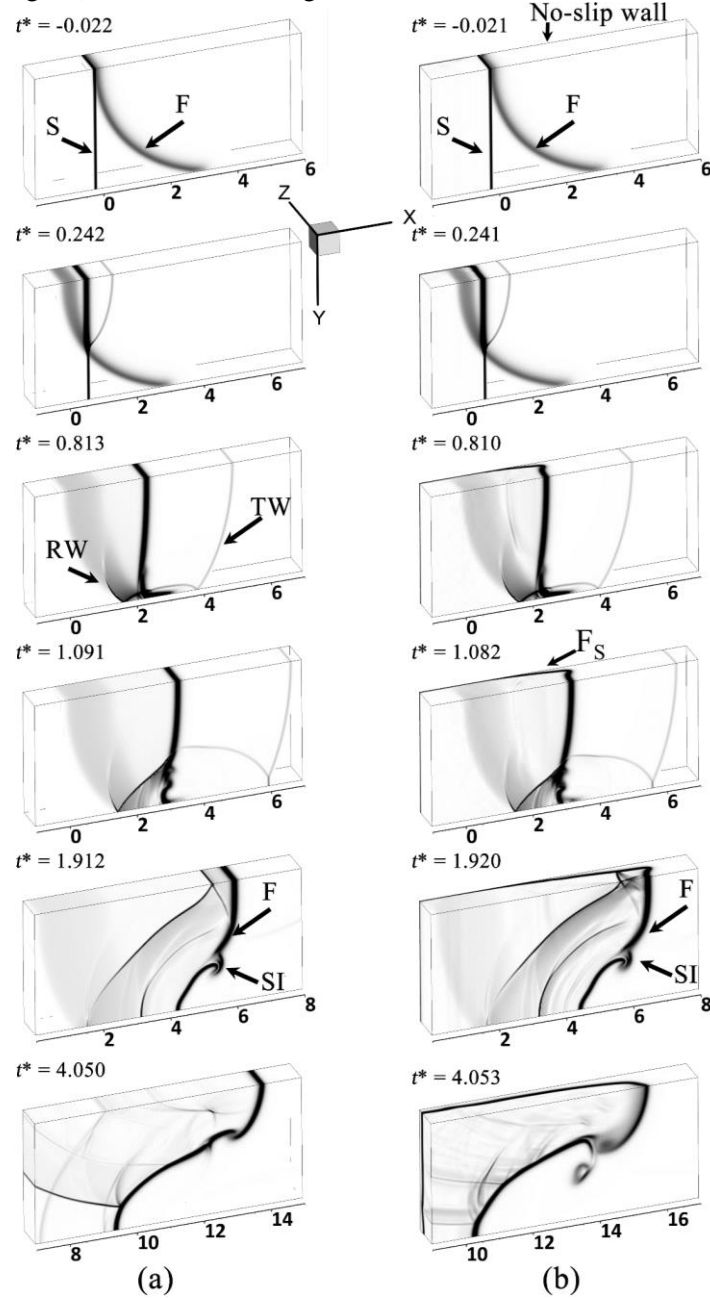


Figure 4. Time sequence of computed 3D schlieren-type images in the case of (a) free-slip BCs and (b) no-slip BCs. The letters indicate the incident shock (S), the flame (F), the reflected waves (RW), and the transmitted waves (TW), secondary instability (SI), stretched flame front ($F_S$). Here, $t^* = t/(\eta_0/V_S)$ is the normalized time.

The flame shows different distortions in the *z*-direction. In the free-slip case, the initially steady flame is flattened in the *x*-direction as the shock wave penetrates, as shown at $t^* = 0.242$ in Fig. 4a. The flame amplitude is reduced to a minimum value in *x*-direction at the end of stage $S_1$ ($t^* = 1.091$), as shown in Fig. 4a. As the flame perturbation enters stage $S_2$, the flame front evolves into a funnel-shaped interface and appears as a classical RMI structure, as shown at $t^* = 1.912$. As the perturbation continues to grow, the flame develops a very long neck (see $t^* = 4.050$). The flame impacted by a shock wave in the free-slip case here can be considered to be a 2D case. In the no-slip case, the two-dimensional perturbation is broken and the dynamical process becomes three-dimensional because of the presence of wall friction. The flame is significantly stretched, consequently leading to rapid growth of global flame perturbation, as shown at $t^* = 0.810$. The flame continues to be stretched after the shock wave in stage $S_2$, causing a significantly large global flame perturbation, as shown at 4.053.

## 3.2 Perturbation growth rate

Figure 5 shows the normalized amplitude of the flame perturbation ($\eta/\eta_0$) as a function of normalized time in a comparison between numerical simulations with different wall BCs and the theory by Meyer and Blewett [12]. For the free-slip case, the amplitude of flame perturbation at the slice of $z = 0$ $\eta$ is given here since it is equivalent to a 2D perturbation, while for the no-slip case, the maximum flame amplitude $\eta_{max}$ is measured in addition to that at $z = 0$ ($\eta$). The measurements of flame amplitudes were illustrated in Section 2.
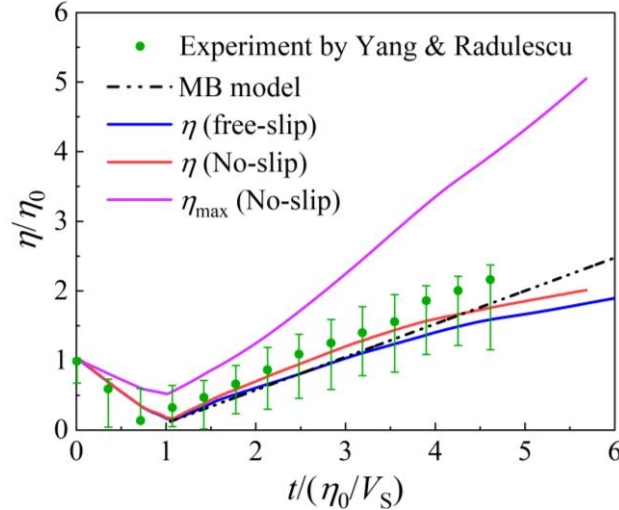


Figure 5. Normalized amplitudes of flame perturbation as a function of normalized time in the numerical simulations, experiment by Yang and Radulescu [19] and theory of Meyer and Blewett [12].

The perturbation growth in stage $S_2$ starts shortly after the incident shock completely leaves the flame at about $t^* = 1.091$ and 1.082 for the free-slip and no-slip cases, respectively. The global perturbation $\eta_{max}$ starts to increase around $t^* = 1.016$ in the no-slip case, as shown in Fig. 5. Previous studies [17, 58] suggest that growth of flame perturbation in early stages is dominated by the inert RMI because the time scale for RMI is significantly shorter than that for chemical reactions. The evolution of RMI can be considered linear when amplitude satisfies $\eta k < 1$ ($k = 2\pi/\lambda$ is the wave number of the perturbation) [12, 26, 31, 59]. Here, we compare the perturbation growth of flame with the linear model of RMI proposed by Meyer and Blewett (MB model) [12],

$$\frac{d\eta}{dt} = k \frac{\eta^+ + \eta_0}{2} \Delta u A^+,$$ (12)

where $\Delta u$ – the flame speed imparted by the shock, m/s; $A^+ = (\rho_1 - \rho_2)/(\rho_1 + \rho_2)$ – post-shock Atwood number, $\eta^+$ – perturbation amplitude after shock passage, cm.

Both the growth rates of flame perturbation $\eta$ at stage $S_2$ in the two cases of different wall BCs show a good agreement with that of MB model, as shown in Fig. 5. However, the growth rate of

global flame perturbation is significantly larger in the no-slip case than that in the free-slip case in both the compression and perturbation growth stages due to the flame stretching near the no-slip wall. Note that even at $z = 0$ slice, the perturbation starts to grow slightly faster in the perturbation growth stage in the no-slip case. This implies that the entire flame is influenced by the wall friction in the growth stage.

**3.3 Effect of wall friction on the shock-flame interactions**

3.3.1 Flame stretch

Wall friction can lead to the development of non-uniform flow that stretches the flame, increases flame surface and thus causes flame acceleration [42, 43]. To estimate the influence of wall friction on the shock-flame interaction, the flame stretch caused by the non-uniform flow is discussed here. This stretch rate can be calculated as [36, 60],

$$\kappa_s = (\delta_{ij} - n_i n_j) \frac{\partial u_i}{\partial x_j}, \tag{13}$$

where $n_i$ – the $i$th component of the unit vector normal to the flame surface.
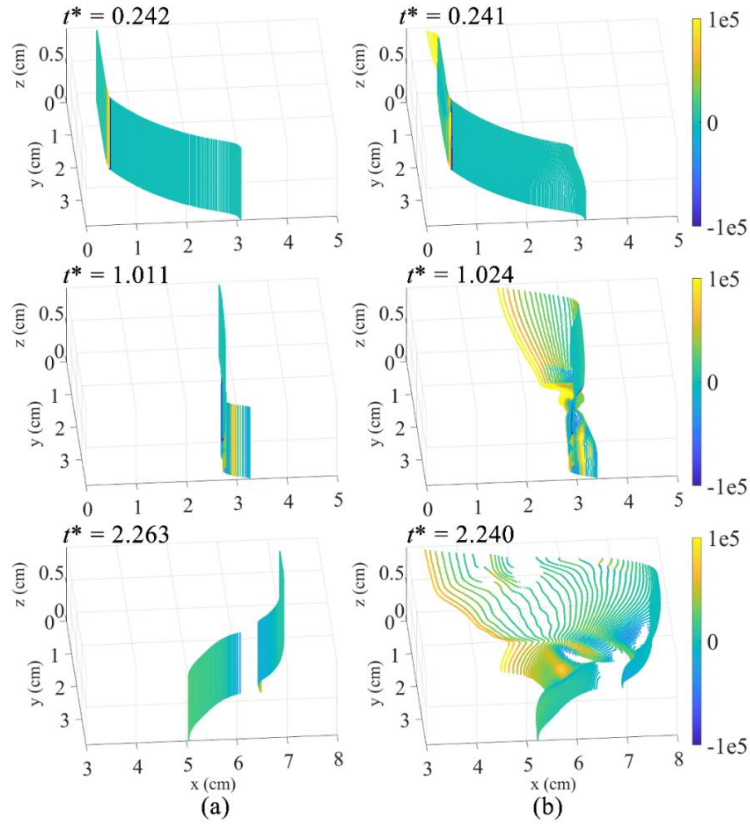


Figure 6. Tangential stretch rate $\kappa_s$ at the flame surface where $Y = 0.5$ during the process of shock-flame interactions in the (a) free-slip and (b) no-slip cases.

Figure 6 shows the calculated stretch rate $\kappa_s$ at the flame surface (iso-surface where $Y = 0.5$) during the process of shock-flame interactions in the two cases. In the free-slip case, the flame is stretched at the intersection of shock and flame with $\kappa_s \sim 10^5$, while the rest of the flame is only weakly stretched with $\kappa_s \sim 0$, as shown at $t^* = 0.242$ and $1.011$ in Fig. 6a. After the shock passes the flame, the entire flame is weakly stretched with $\kappa_s \sim 0$, as shown at $t^* = 2.263$ in Fig. 6a. In the no-slip case, the flame is significantly stretched with $\kappa_s \sim 10^5$ in the near-wall region by the non-uniform flow induced by the interactions between shock and wall friction, see at $t^* = 0.241$ and $1.024$ in Fig. 6b.

7

The flame continues to be stretched by the non-uniform flow near the no-slip wall even after the shock penetrates the flame, see at $t^* = 2.240$ in Fig. 6b.

3.3.2 Damping of local flame perturbation close to the no-slip wall

Previous studies suggested that baroclinic vorticity generation resulting from the misalignment of the pressure gradient of the shock with the density gradient across the interface (flame) leads to the development of RMI on the interface (flame) [25, 28, 29]. Thus, we aslo discuss the effect of wall friction on shock-flame interactions in terms of vorticity dynamics. Figure 7 shows the vorticity fields near the flame front at the slices of $z = 0$ and $z = 0.98L_z$ (very close to the free-slip or no-slip wall) in the two cases of different wall BCs in the perturbation growth stage. Here, we display the vorticity in $z$-direction considering the direction of cross product of density and pressure $\nabla \rho \times \nabla p$.
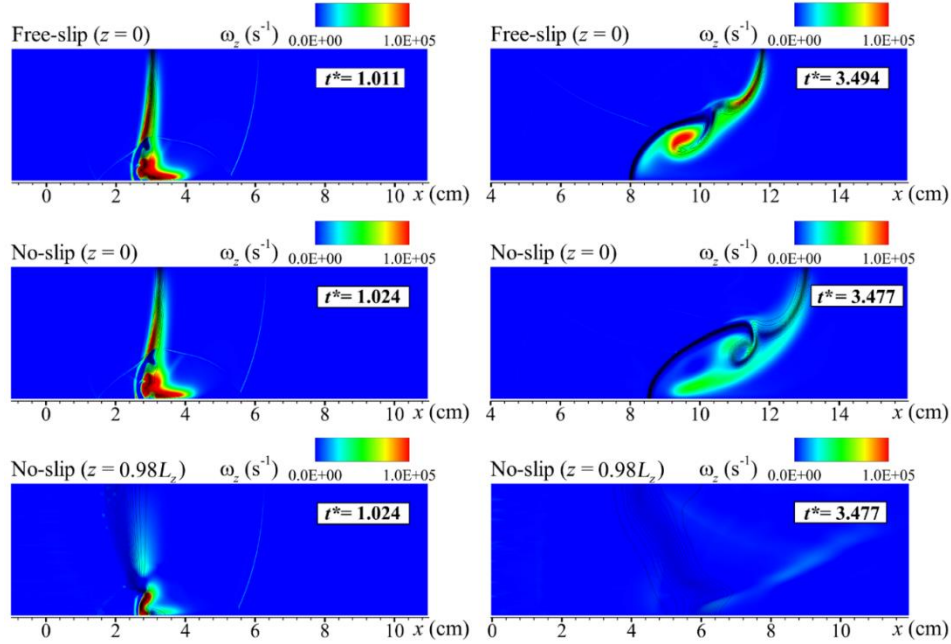


Figure 7. Fields of vorticity in $z$-direction $\omega_z$ at different $z$-slices in the cases of two wall BCs. The black lines are the contours of unburned mass fraction.

It can be found that the difference of $z$-vorticity deposited on flame at $z = 0$ slice is minor (e.g., $t^* = 1.011$ or 1.024 in Fig. 7) although it is affected to some extent by the wall friction (Fig. 6). This explains the similar growth rates in the two cases at $z = 0$, as shown in Fig. 5. The vorticity in $z$-direction localized on flame in close proximity to the no-slip wall ($z = 0.98L_z$) slice is much less than that at $z = 0$ in the no-slip case. The difference in the vorticity deposition on the flame in $z$-direction at different $z$-slices leads to the non-uniform perturbation evolution. This effect and the flame stretching due to wall friction ultimately cause a significantly higher perturbation growth rate in the no-slip case (Fig. 5).

To quantify the difference in the magnitude of vorticity in $z$-direction, here we discuss vortex transport terms in the vortex balance equation to approach it. The vorticity balance equation can be derived by the curl of the momentum equation [32, 33],

$$\frac{\partial \omega_i}{\partial t} + u_k \frac{\partial \omega_i}{\partial x_k} = \underbrace{\omega_k \frac{\partial u_i}{\partial x_k}}_{T_1} \underbrace{- \varepsilon_{ijk} \frac{1}{\rho} \frac{\partial \rho}{\partial x_j} \left( \frac{\partial \tau_{kl}}{\partial x_l} \right)}_{T_2} + \underbrace{\frac{\varepsilon_{ijk}}{\rho} \left( \frac{\partial^2 \tau_{kl}}{\partial x_j \partial x_l} \right)}_{T_3} \underbrace{- \omega_i \frac{\partial u_k}{\partial x_k}}_{T_4} + \underbrace{\frac{1}{\rho^2} \varepsilon_{ijk} \frac{\partial \rho}{\partial x_j} \frac{\partial p}{\partial x_k}}_{T_5}, \quad (14)$$

where, $\omega_i = \varepsilon_{ijk} \partial u_k / \partial x_j$ is the $i$th component of the vorticity, $\varepsilon_{ijk}$ is the permutation tensor.

The left-hand side of Eq. (12) is the rate of the variation of vorticity in a Lagrangian packet of fluid. The first term on the right ($T_1$) is the vortex stretching term; the second term ($T_2$) is the viscous torque term due to the misalignment between the gradients of viscous stress and density; the third term ($T_3$) describes the viscous dissipation; the fourth term ($T_4$) denotes the vorticity destruction by dilation;

the last term ($T_5$) is the baroclinic torque term that is responsible for inducing RMI in shock-flame interactions.

Figure 8 shows the area integrals of each transport term ($T_m$, $m = 1{\sim}5$) for $z$-vorticity $\omega_z$ at the flame at different $z$-slices in the free-slip and no-slip cases. During the shock-flame interactions, vorticity is generated by baroclinic term and then amplified by the dilation term. These two terms are up to $\sim 10^5$ in both cases, as shown in Fig. 8. The wall friction makes a difference to vortex dynamics by the terms of vortex stretching $T_1$, viscous torque $T_2$, and viscous dissipation $T_3$. At $z = 0$ slice, it is shown that the magnitude of these three terms is very small and can be neglected, compared to the baroclinic and dilation terms in both cases, as shown in Fig. 8a and b. At $z = 0.98L_z$ slice, the vortex stretching term has a positive contribution to the vorticity generation, whereas both the viscous torque and the viscous dissipation have considerable negative effects, as shown in Fig. 8c. The net contribution of these three terms is negative and partially cancels out the last two terms ($T_4$ and $T_5$), leading to a lower magnitude of vorticity in z-direction deposited on flame.
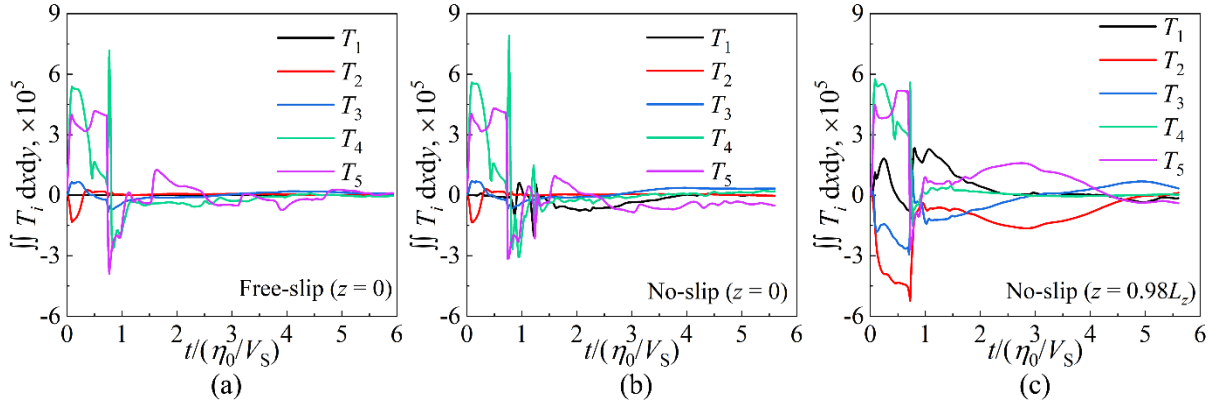


Figure 8. Integral of vortex transport terms at of the flame at different $z$-slice as a function of time in the two case of different wall boundary conditions.

## 4 CONCLUSIONS

Multi-dimensional shock-flame interactions were investigated by solving the three-dimensional (3D) fully-compressible reactive Navier-Stokes equations coupled to a single-step chemistry model using a fifth-order scheme on a dynamically adapting grid in this paper. The thermochemical parameters were calibrated to reproduce the properties of the combustion waves in a stoichiometric hydrogen-air mixture. Two types of wall boundary conditions (free-slip/no-slip) on the sidewall of the domain were adopted to examine the effect of wall friction on the shock-flame interaction. Overall, the numerical simulations showed flame perturbation growth similar to experiment observation and theory prediction [12].

The results show that wall friction has a significant influence on the shock-flame interaction and flame perturbation growth. In general, the flame perturbation during shock-flame interaction can be divided into two stages, i.e., shock compression ($S_1$) and perturbation growth stages ($S_2$). The effect of wall friction leads to more drastic flame deformation in both stages in the no-slip case, especially in stage $S_2$. For the free-slip case, the perturbation development as well as the flame dynamics in stage $S_2$ is dominated by the Richtmyer-Meshkov instability (RMI) induced by the shock. For the no-slip case, the flame perturbation is not only promoted through RMI but also strongly enhanced by the stretching effect of wall friction, and thus the growth rate of global perturbation is much higher than that in the free-slip case.

Two effects of wall friction on flame-shock interaction are concluded: (1) flame stretching, and (2) damping of local flame perturbation very close to the no-slip wall. The flame stretch effect leads to non-uniform development of the perturbated flame and thus a significantly higher growth rate in global flame perturbation in the no-slip case compared to the free-slip case. By contrast, the damping effect locally moderates the flame perturbation in close proximity to the no-slip wall because less vorticity is deposited on this part of flame.

9

## ACKNOWLEDGEMENTS

## REFERENCES

[1] Poludnenko, A.Y., Chambers, J., Ahmed, K., Gamezo, V.N., Taylor, B.D., A unified mechanism for unconfined deflagration-to-detonation transition in terrestrial chemical systems and type Ia supernovae, *Science,* **366**, No. 6465, 2019, pp. eaau7365.

[2] Jha, S.W., Maguire, K., Sullivan, M., Observational properties of thermonuclear supernovae, *Nature Astronomy,* **3**, No. 8, 2019, pp. 706-716.

[3] Seitenzahl, I.R., Ghavamian, P., Laming, J.M., Vogt, F., Optical Tomography of Chemical Elements Synthesized in Type Ia Supernovae, *Physical Review Letters,* **123**, No. 4, 2019, pp. 041101.041101-041101.041106.

[4] Oran, E.S., Understanding explosions – From catastrophic accidents to creation of the universe, *Proceedings of the Combustion Institute,* **35**, No. 1, 2015, pp. 1-35.

[5] Wolański, P., Detonative propulsion, *Proceedings of the Combustion Institute,* **34**, No. 1, 2013, pp. 125-158.

[6] Marble, F.E., Hendricks, G.J., Zukoski, E.E. Progress Toward Shock Enhancement of Supersonic Combustion Processes. In: editor^editors. Turbulent Reactive Flows. 1989; New York, NY: Springer US. p. 932-950.

[7] Yang, Q., Chang, J., Bao, W., Richtmyer-Meshkov Instability Induced Mixing Enhancement in the Scramjet Combustor with a Central Strut, *Advances in Mechanical Engineering,* **6**, 2014, pp. 614189.

[8] Oran, E.S., Chamberlain, G., Pekalski, A., Mechanisms and occurrence of detonations in vapor cloud explosions, *Progress in Energy and Combustion Science,* **77**, 2020, pp. 100804.

[9] Oran, E.S., Gamezo, V.N., Zipf, R.K., Large-Scale Experiments and Absolute Detonability of Methane/Air Mixtures, *Combustion Science and Technology,* **187**, No. 1-2, 2015, pp. 324-341.

[10] Xiao, H., Duan, Q., Sun, J., Premixed flame propagation in hydrogen explosions, *Renewable and Sustainable Energy Reviews,* **81**, 2018, pp. 1988-2001.

[11] Markstein, G.H., A shock-tube study of flame front-pressure wave interaction, *Proceedings of the Combustion Institute,* **6**, No. 1, 1957, pp. 387-398.

[12] Meyer, K.A., Blewett, P.J., Numerical Investigation of the Stability of a Shock-Accelerated Interface between Two Fluids, *The Physics of Fluids,* **15**, No. 5, 1972, pp. 753-759.

[13] Khokhlov, A.M., Oran, E.S., Chtchelkanova, A.Y., Wheeler, J.C., Interaction of a shock with a sinusoidally perturbed flame, *Combustion and Flame,* **117**, No. 1, 1999, pp. 99-116.

[14] Khokhlov, A.M., Oran, E.S., Thomas, G.O., Numerical simulation of deflagration-to-detonation transition: the role of shock–flame interactions in turbulent flames, *Combustion and Flame,* **117**, No. 1–2, 1999, pp. 323-339.

[15] Scarinci, T., Lee, J.H., Thomas, G.O., Bambrey, R., Edwards, D.H., Amplification of a Pressure Wave by Its Passage Through a Flame Front, Dynamics of Heterogeneous Combustion and Reacting Systems, American Institute of Aeronautics and Astronautics1993, pp. 3-24.

[16] Thomas, G., Bambrey, R., Brown, C., Experimental observations of flame acceleration and transition to detonation following shock-flame interaction, *Combustion Theory and Modelling,* **5**, No. 4, 2001, pp. 573-594.

[17] Yang, H., Radulescu, M.I., Dynamics of cellular flame deformation after a head-on interaction with a shock wave: reactive Richtmyer–Meshkov instability, *Journal of Fluid Mechanics,* **923**, 2021.

[18] Maxwell, B., Pekalski, A., Radulescu, M., Modelling of the transition of a turbulent shock-flame complex to detonation using the linear eddy model, *Combustion and Flame,* **192**, 2018, pp. 340-357.

[19] Bakalis, G., Tang-Yuk, K.C., Mi, X., Nikiforakis, N., Ng, H.D., Numerical simulation of deflagration-to-detonation transition via shock–multiple flame kernels interactions, *Computers & Mathematics with Applications,* **83**, 2021, pp. 111-126.

[20] Yang, H., Radulescu, M.I., Enhanced DDT mechanism from shock-flame interactions in thin channels, *Proceedings of the Combustion Institute,* **38**, No. 3, 2021, pp. 3481-3495.

[21] Oran, E.S., Gamezo, V.N., Origins of the deflagration-to-detonation transition in gas-phase combustion, *Combustion and Flame,* **148**, No. 1, 2007, pp. 4-47.

[22] Ciccarelli, G., Johansen, C.T., Parravani, M., The role of shock–flame interactions on flame acceleration in an obstacle laden channel, *Combustion and Flame,* **157**, No. 11, 2010, pp. 2125-2136.

[23] Goodwin, G.B., Houim, R.W., Oran, E.S., Shock transition to detonation in channels with obstacles, *Proceedings of the Combustion Institute,* **36**, No. 2, 2017, pp. 2717-2724.

[24] Houim, R.W., Ozgen, A., Oran, E.S., The role of spontaneous waves in the deflagration-to-detonation transition in submillimetre channels, *Combustion Theory and Modelling,* **20**, No. 6, 2016, pp. 1068-1087.

[25] Ju, Y., Shimano, A., Inoue, O., Vorticity generation and flame distortion induced by shock flame interaction, *Proceedings of the Combustion Institute,* **27**, No. 1, 1998, pp. 735-741.

[26] Richtmyer, R.D., Taylor instability in shock acceleration of compressible fluids, *Communications on Pure and Applied Mathematics,* **13**, No. 2, 1960, pp. 297-319.

[27] Meshkov, E.E., Instability of the interface of two gases accelerated by a shock wave, *Fluid Dynamics,* **4**, No. 5, 1969, pp. 101-104.

[28] Hawley, J.F., Zabusky, N.J., Vortex paradigm for shock-accelerated density-stratified interfaces, *Physical Review Letters,* **63**, No. 12, 1989, pp. 1241-1244.

[29] Zabusky, N.J., VORTEX PARADIGM FOR ACCELERATED INHOMOGENEOUS FLOWS: Visiometrics for the Rayleigh-Taylor and Richtmyer-Meshkov Environments, *Annual Review of Fluid Mechanics,* **31**, No. 1, 1999, pp. 495-536.

[30] Zhou, Y., Rayleigh–Taylor and Richtmyer–Meshkov instability induced flow, turbulence, and mixing. I, *Physics Reports,* **720-722**, 2017, pp. 1-136.

[31] Zhou, Y., Williams, R.J.R., Ramaprabhu, P., Groom, M., Thornber, B., Hillier, A., Mostert, W., Rollin, B., Balachandar, S., Powell, P.D., Mahalov, A., Attal, N., Rayleigh–Taylor and Richtmyer–Meshkov instabilities: A journey through scales, *Physica D: Nonlinear Phenomena,* **423**, 2021, pp. 132838.

[32] Lipatnikov, A.N., Nishiki, S., Hasegawa, T., A direct numerical simulation study of vorticity transformation in weakly turbulent premixed flames, *Physics of Fluids,* **26**, No. 10, 2014, pp. 105104.

[33] Bambauer, M., Chakraborty, N., Klein, M., Hasslberger, J., Vortex dynamics and fractal structures in reactive and nonreactive Richtmyer–Meshkov instability, *Physics of Fluids,* **33**, No. 4, 2021, pp. 044114.

[34] Mikaelian, Karnig, O., Explicit expressions for the evolution of single-mode Rayleigh-Taylor and Richtmyer-Meshkov instabilities at arbitrary Atwood numbers, *Physical Review E Statistical Nonlinear & Soft Matter Physics,* **67**, No. 2, 2003, pp. 026319.

[35] Marra, F.S., Continillo, G., Numerical study of premixed laminar flame propagation in a closed tube with a full navier-stokes approach, *Symposium (International) on Combustion,* **26**, No. 1, 1996, pp. 907-913.

[36] Thierry, P., Veynante, D., Theoretical and numerical combustion. Third Edition, 2012.

[37] Houim, R.W., Kuo, K.K., A low-dissipation and time-accurate method for compressible multi-component flow with variable specific heat ratios, *Journal of Computational Physics,* **230**, No. 23, 2011, pp. 8527-8553.

[38] Gamezo, V.N., Khokhlov, A.M., Oran, E.S., The influence of shock bifurcations on shock-flame interactions and DDT, *Combustion and Flame,* **126**, No. 4, 2001, pp. 1810-1826.

[39] Gamezo, V.N., Oran, E.S., Khokhlov, A.M., Three-dimensional reactive shock bifurcations, *Proceedings of the Combustion Institute,* **30**, No. 2, 2005, pp. 1841-1847.

[40] Li, X., Xiao, H., Duan, Q., Sun, J., Numerical study of premixed flame dynamics in a closed tube: Effect of wall boundary condition, *Proceedings of the Combustion Institute,* **38**, No. 2, 2021, pp. 2075-2082.

[41] Shen, T., Xiao, H.H., Numerical study of the stability of premixed flames propagating in half-open tubes, *Combustion Theory and Modelling,* **26**, No. 4, 2022, pp. 774-795.

[42] Akkerman, V.Y., Bychkov, V., Petchenko, A., Eriksson, L.E., Accelerating flames in cylindrical tubes with nonslip at the walls, *Combustion and Flame,* **145**, No. 1/2, 2006, pp. 206-219.

[43] Bychkov, V., Petchenko, A., Akkerman, V.y., Eriksson, L.-E., Theory and modeling of accelerating flames in tubes, *Physical Review E,* **72**, No. 4, 2005, pp. 046307.

[44] Xiao, H., Oran, E.S., Flame acceleration and deflagration-to-detonation transition in hydrogen-air mixture in a channel with an array of obstacles of different shapes, *Combustion and Flame,* **220**, 2020, pp. 378-393.

[45] Xiao, H., Houim, R.W., Oran, E.S., Formation and evolution of distorted tulip flames, *Combustion and Flame,* **162**, No. 11, 2015, pp. 4084-4101.

[46] Kaplan, C.R., Özgen, A., Oran, E.S., Chemical-diffusive models for flame acceleration and transition-to-detonation: genetic algorithm and optimisation procedure, *Combustion Theory and Modelling,* **23**, No. 1, 2019, pp. 67-86.

[47] Goodwin, G.B., Oran, E.S., Premixed flame stability and transition to detonation in a supersonic combustor, *Combustion and Flame,* **197**, No. 2018, pp. 145-160.

[48] Goodwin, D.G., Moffat, H.K., Speth, R.L., Cantera: An Object-oriented Software Toolkit for Chemical Kinetics, Thermodynamics, and Transport Processes. Version 2.2.0, 2015.

[49] Burke, M.P., Chaos, M., Ju, Y., Dryer, F.L., Klippenstein, S.J., Comprehensive H2/O2 kinetic model for high-pressure combustion, *International Journal of Chemical Kinetics,* **44**, No. 7, 2012, pp. 444-474.

[50] Gamezo, V.N., Oran, E.S., Flame Acceleration in Narrow Channels: Applications for Micropropulsion in Low-Gravity Environments, *AIAA Journal,* **44**, No. 2, 2006, pp. 329-336.

[51] Xiao, H., Houim, R.W., Oran, E.S., Effects of pressure waves on the stability of flames propagating in tubes, *Proceedings of the Combustion Institute,* **36**, No. 1, 2017, pp. 1577-1583.

[52] Gamezo, V.N., Vasil'Ev, A.A., Khokhlov, A.M., Oran, E.S., Fine cellular structures produced by marginal detonations, *Proceedings of the Combustion Institute,* **28**, No. 1, 2000, pp. 611-617.

[53] Kessler, D.A., Gamezo, V.N., Oran, E.S., Multilevel detonation cell structures in methane-air mixtures, *Proceedings of the Combustion Institute,* **33**, No. 2, 2011, pp. 2211-2218.

[54] Xiao, H., Oran, E.S., Shock focusing and detonation initiation at a flame front, *Combustion and Flame,* **203**, No. 2019, pp. 397-406.

[55] Gamezo, V.N., Bachman, C.L., Oran, E.S., Flame acceleration and DDT in large-scale obstructed channels filled with methane-air mixtures, *Proceedings of the Combustion Institute,* **38**, No. 3, 2021, pp. 3521-3528.

[56] Toro, E.F., Spruce, M., Speares, W., Restoration of the contact surface in the HLL-Riemann solver, *Shock Waves,* **4**, No. 1, 1994, pp. 25-34.

[57] Boxlib. Center for computational sciences and engineering, University of California, Berkeley, December 2015 http://boxlib-codes.github.io/.

[58] Jiang, H., Dong, G., Chen, X., Li, B., A parameterization of the Richtmyer–Meshkov instability on a premixed flame interface induced by the successive passages of shock waves, *Combustion and Flame,* **169**, 2016, pp. 229-241.

[59] Vandenboomgaerde, M., Mügler, C., Gauthier, S., Impulsive model for the Richtmyer-Meshkov instability, *Physical Review E,* **58**, No. 2, 1998, pp. 1874-1882.

[60] Zhang, F., Zirwes, T., Häber, T., Bockhorn, H., Trimis, D., Suntz, R., Near Wall Dynamics of Premixed Flames, *Proceedings of the Combustion Institute,* **38**, No. 2, 2021, pp. 1955-1964.